RAL-TR-1999-009
January 1999

The process $e^+e^- \to Ht\bar{t}$ and its backgrounds at future electron-positron colliders[1]

S. Moretti†

Rutherford Appleton Laboratory,
Chilton, Didcot, Oxon OX11 0QX, UK.

Abstract

The process $e^+e^- \to Ht\bar{t}$ can be used at the Next Linear Collider to measure the Higgs-top Yukawa coupling. In this paper, we compute $2 \to 8$ processes of the form $e^+e^- \to b\bar{b}b\bar{b}W^+W^- \to b\bar{b}b\bar{b}\ell^\pm\nu_\ell\ q\bar{q}'$, accounting for the Higgs-top-antitop signal as well as several irreducible backgrounds in the semi-leptonic top-antitop decay channel. We restrict ourselves to the case of a light Higgs boson in the range 100 GeV $\lesssim M_H \lesssim$ 140 GeV. We use helicity amplitude techniques to compute exactly such processes at tree level in the framework of the Standard Model. Total rates and differential spectra of phenomenological interest are given and discussed.

[1]Work supported by the UK PPARC.
† Electronic mail: moretti@v2.rl.ac.uk.

At the Next Linear Collider (NLC), running with a centre-of-mass (CM) energy of $\sqrt{s} =$ 500 GeV [1], the Higgs boson of the Standard Model (SM) can be produced in association with top-antitop pairs [2], through the process $e^+e^- \to Ht\bar{t}$, which proceeds via the diagrams displayed in Fig. 1. That is, the scalar particle can be radiated either from the top quark pair or from a virtual Z boson. In the latter case, it is the neutral gauge vector to eventually produce the heavy quark pair. Clearly, given the actual value of the top mass, $m_t \approx 175$ GeV, between the two sets of graphs, it is the first one which dominates. On the one hand, the $Z^* \to t\bar{t}$ decay occurs far off the mass-shell of the Z boson. On the other hand, the large Yukawa coupling exceeds the strength of the HZZ vertex. Indeed, it is the possibility of measuring such Yukawa interaction that renders associated production of Higgs bosons and top (anti)quarks phenomenologically interesting at the NLC [3].

From the above values of $\sqrt{s}$ and m_t, it follows that only Higgs scalars with mass M_H up to 140 GeV or so can be produced, because of the kinematical limit imposed by the difference $\sqrt{s} - 2m_t$. For such values of M_H, the dominant Higgs decay mode is $H \to b\bar{b}$, this being overtaken by the off-shell decay into two $W^{\pm}$'s, i.e., $H \to W^{+*}W^{-*}$, only for $M_H \gtrsim 130 - 140$ GeV, see Fig. 1 of Ref. [4]. However, these Higgs masses are extremely close to the kinematical limit of the $Ht\bar{t}$ intermediate state, so that the production cross section of the latter is very small [5]. Furthermore, notice that in order to reconstruct the Higgs mass one would require a fully hadronic decay of the $W^{+*}W^{-*}$ pairs produced in the Higgs decay, this leading to a signature with at least eight jets in the final state. In fact, at least one top quark would be required to decay into jets, in order to exploit the reconstruction of its mass to reduce various QCD backgrounds. In other terms, the search for $H \to W^{+*}W^{-*}$ decays from $e^+e^- \to Ht\bar{t}$ would be of difficult experimental use, considering the reduced number of events, the rather chaotic topology and the problem that the latter generates, because of the combinatorics, while attempting to disentangle the H and t resonances. In the end, one would be much better off to rely on the two-body mode $H \to b\bar{b}$ over the entire M_H range allowed by Higgs-top-antitop intermediate states at $\sqrt{s} = 500$ GeV.

As for $t\bar{t}$ decays, one would most likely exploit the semi-leptonic channel, i.e., $t\bar{t} \to b\bar{b}W^+W^- \to b\bar{b}\ell^{\pm}\nu_\ell\, q\bar{q}'$, where ℓ and ν represent a lepton at high transverse momentum (to be used for triggering purposes) and its companion neutrino and $q\bar{q}'$ refers to the two possible combinations of light quark pairs and their charge conjugated channels (neglecting Cabibbo-Kobayashi-Maskawa mixing effects). This is the decay signature we will concentrate on. As a matter of fact, such a choice is not restrictive, in the sense that the latter is to date the experimentally preferred channel in searching for $t\bar{t} \to b\bar{b}W^+W^-$ events [6].

If one does assume such Higgs and top decay modes, then signal events can be searched for in data samples made up by four b quark jets, two light quark jets, a lepton and a neutrino. In other terms, a '$4b + 2$ jets $+ \ell^{\pm} + E_{\rm miss}$' signal, assuming the four heavy quark jets to be recognised as such thanks to the μ-vertex devices of the NLC, with $\ell = e, \mu, \tau$[2] and where the missing energy, $E_{\rm miss}$, originates from the neutrino escaping detection.

Though the calculation of the on-shell production $e^+e^- \to Ht\bar{t}$ has been tackled long ago [7], that of the complete $2 \to 8$ body reaction, without any factorisation of production and decay processes, has never been attempted before. Not surprisingly so, as even in presence of only five diagrams, both the large number of particles in the final state and the complicate

[2]We include τ's to enhance the signal rate, assuming that they are distinguishable from quark jets.

resonant structure of the latter impose non-trivial problems to the matrix element (ME) calculation and to its integration over the phase space, respectively. Things become even more involved if one starts including (irreducible) backgrounds in the calculation, as needed in order to realistically simulate phenomenological studies. For example, if one restricts oneself to all those channels that proceed through an intermediate $Hb\bar{b}W^+W^-$ stage, then the full gauge invariant set (including Higgs bosons produced via other graphs than those in Fig. 1) counts 350 tree-level diagrams.

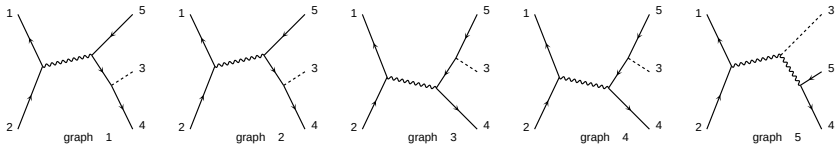


Figure 1: Relevant Feynman diagrams contributing at lowest order to the process $e_1^+e_2^- \to H_3t_4\bar{t}_5$. An internal wavy line represents a γ (graphs 1, 3) or a Z (graphs 2, 4, 5).

One of the main irreducible backgrounds to the Higgs-top-antitop signal at the NLC is the scattering $e^+e^- \to Zt\bar{t}$ [8], if one considers that the two processes have comparable production cross sections [2, 8] and that the Z boson decays into $b\bar{b}$ pairs some 15% of the times. Even though the difference between M_H and M_Z is always larger than 10 GeV (assuming a late 100 GeV bound on the former from the all of LEP2 data [9]) and the width of the Higgs boson is very narrow (about ten MeV at the most for masses up to 140 GeV, see Fig. 2 of Ref. [4]), one should recall both the large value of that of the Z boson, $\Gamma_Z \approx 2.5$ GeV, the finite efficiency of the detectors in reconstructing jet energies and directions (to say the least, yielding a resolution of some 5 GeV in invariant mass) and the mis-assignment problems arising when pairing the four b jets in the final state in the attempt to recognise resonances in the $b\bar{b}$ decay channel. Thus, it is inevitable to conclude that $Zt\bar{t}$ events will represent a serious noise. On-shell Z-top-antitop production proceeds at tree-level through the nine graphs of Fig. 2. If one however considers, on the same footing as was done for Higgs production, all the gauge invariant set of amplitudes producing $Zb\bar{b}W^+W^-$ intermediate states, followed by $Z \to b\bar{b}$, then the number of graphs involved is 546. (Notice that several of the production channels described by the latter do involve Higgs bosons, some of which decay into $b\bar{b}$ pairs.)

In addition, one should also consider $e^+e^- \to gb\bar{b}W^+W^-$ intermediate states, where g represents a gluon eventually yielding $b\bar{b}$ pairs. Although none of $b\bar{b}$ invariant masses has in this case the tendency of being produced around M_H (in particular, the one induced by the g splitting logarithmically increases at very low mass values, because of the infrared singularity of QCD, only regulated by the b mass, m_b), such mechanisms proceed through strong interactions, so that their production rates could well be comparable to those of the signal[3]. In fact, because of the mis-pairings of b quarks, large tails in the $b\bar{b}$ invariant mass distributions could arise, despite of the softness and collinearity of two of the heavy quarks. The dominant background contribution from these mechanisms would come from $e^+e^- \to gt\bar{t}$ events [10], with the gluon radiated before the (anti)top decays take place. There are four

[3]For opposite reasons, one can avoid studying $e^+e^- \to \gamma b\bar{b}W^+W^-$ reactions, with the photon splitting into $b\bar{b}$ pairs.

tree-level diagrams associated with this $2 \to 3$ process, see Fig. 3. The total number of those yielding $gb\bar{b}W^+W^-$ states is instead 152.

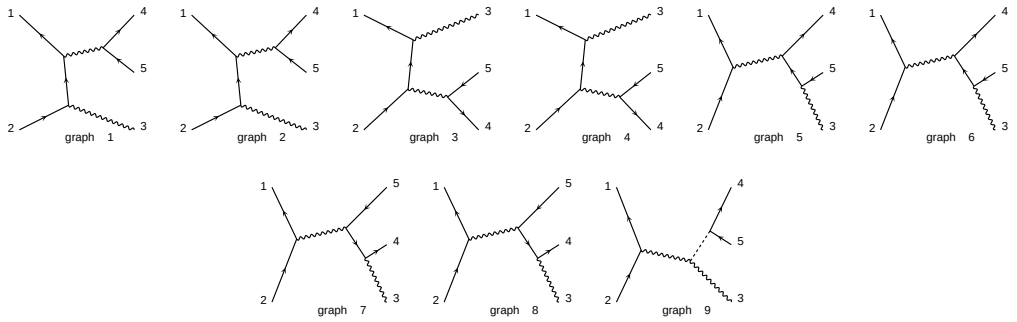


Figure 2: Relevant Feynman diagrams contributing at lowest order to the process $e_1^+e_2^- \to Z_3t_4\bar{t}_5$. An internal wavy line represents a γ (graphs 1, 3, 5, 7) or a Z (graphs 2, 4, 6, 8, 9).

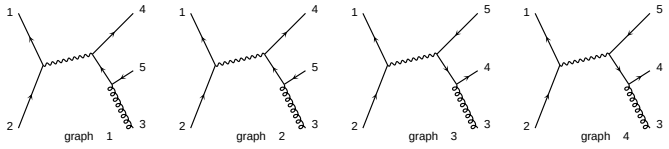


Figure 3: Relevant Feynman diagrams contributing at lowest order to the process $e_1^+e_2^- \to g_3t_4\bar{t}_5$. An internal wavy line represents a γ (graphs 1, 3) or a Z (graphs 2, 4).

It is the purpose of this letter to compute all such processes and compare the signal rates and distributions to those obtained from the various backgrounds that we have described, in order to assess the chances of genuinely exploiting the Higgs-top-antitop production process in measuring the Higgs-top Yukawa coupling. In this respect, the reader should notice one subtlety. In fact, the mentioned coupling not only appears in the $e^+e^-Ht\bar{t} \to Hb\bar{b}W^+W^-$ 'signal', but also in several 'background' mechanisms, such as in $e^+e^- \to W^{\pm *}W^{\mp}$ production with one of bosons off-shell, followed by $W^{\pm *} \to Ht\bar{b} + H\bar{t}b \to Hb\bar{b}W^{\pm}$ and $e^+e^- \to t^*\bar{b}W^-$ production of an off-shell t quark, eventually yielding $t^* \to Ht \to HbW^+$ (plus the charged conjugate case). These can be regarded as 'single top' processes, as opposed to the 'double top' one, i.e., $e^+e^- \to Ht\bar{t}$, themselves being proportional to the Higgs-top Yukawa coupling. More correctly then, these two subprocesses should be considered as additional contributions to the, say, 'Yukawa' signal, further recalling that they carry one resonant top decay (we are selecting the semi-leptonic channel, thus implicitly assuming that no more than one top mass can in principle be reconstructed).

To compute all signal[4] and background graphs we have resorted to helicity amplitudes methods. In particular, we have made use of the `HELAS` subroutines [12], based on the formalism of Ref. [13]. All the `FORTRAN` codes produced this way have been tested for gauge invariance satisfactorily, so to give us confidence in our numerical results. Furthermore,

[4]Note that we calculate the Higgs-top-antitop signal at the leading-order (LO), though we are aware that several higher order corrections (mainly to the on-shell production) are known to date [5, 11]. We do this for consistency, as all the $2 \to 8$ background processes are evaluated here at tree level.

the $2 \to 8$ 'dominant' (as we shall see below) signal and background processes of the form $e^+e^- \to X b\bar{b} W^+W^- \to b\bar{b}b\bar{b}\ell^\pm\nu_\ell q\bar{q}'$, with $X = H, Z$ and g, have also been implemented by using the spinor techniques described in Refs. [14, 15]. Wherever the two approaches overlapped, we have seen perfect agreement between the outputs of the two sets of codes.

Numerical results have been produced after integration of the Feynman amplitudes squared over eight-body phase spaces. In order to account accurately for all their components, we have split the MEs of the form $e^+e^- \to X b\bar{b} W^+W^- \to b\bar{b}b\bar{b}\ell^\pm\nu_\ell q\bar{q}'$ in resonant sub-terms and integrated each of these separately. Only in the end the various integrals were summed up, in order to recover gauge-invariance [16]. The algorithms used to perform the multi-dimensional integrations were `VEGAS` [17] and, for comparison, `RAMBO` [18].

To describe the vector and axial couplings of the gauge bosons to the fermions, we have used $\sin^2\theta_W = 0.2320$. The strong coupling constant α_s entering the QCD processes (i.e., $X = g$) has been evaluated at two loops, with $N_f = 4$ and $\Lambda_{\overline{\rm MS}} = 230$ MeV, at a scale equal to the collider CM energy, $\sqrt{s} = E_{\rm ecm} = 500$ GeV. The electromagnetic coupling was $\alpha_{em} = 1/128$. For masses and widths, we have used: $m_\ell = m_{\nu_\ell} = m_u = m_d = m_s = m_c = 0$, $m_b = 4.25$ GeV, $m_t = 175$ GeV (as default), $M_Z = 91.19$ GeV, $\Gamma_Z = 2.50$ GeV, $M_W = 80.23$ GeV and $\Gamma_W = 2.08$ GeV. As for the top width Γ_t, we have used the LO value of 1.5 GeV. Only in one circumstance, in order to study the sensitivity of the signal processes to the Higgs-top Yukawa coupling, we have changed m_t by ± 5 GeV. The widths corresponding to these two new values are 1.3 and 1.6, for the lower and higher m_t figure, respectively.

Concerning the Higgs boson, we have spanned its mass M_H over the range 100 to 140 GeV. As for its width, Γ_H, we have computed it by means of the same program described in Ref. [4], which uses a running b mass in evaluating the $H \to b\bar{b}$ decay fraction. Thus, for consistency, we have evolved here the value of m_b entering the Hbb Yukawa coupling of the $H \to b\bar{b}$ decay current in the same way as then.

Finally, notice that starting from our $2 \to 8$ MEs for $e^+e^- \to X t\bar{t} \to b\bar{b}b\bar{b}W^+W^- \to b\bar{b}b\bar{b}\ell^\pm\nu_\ell q\bar{q}'$, in all cases $X = H, Z$ and g, we are able to reproduce (apart from minor spin correlations) the cross sections that one obtains from the $2 \to 3$ ones for $e^+e^- \to X t\bar{t}$, times the relevant branching ratios (BRs), by adopting a Narrow Width Approximation (NWA) for the various resonances R involved (i.e., $R = H, t, W^\pm$ and Z), by rewriting the corresponding (denominator of the) propagators as (for $\Gamma \equiv \Gamma_R$ the standard expression is recovered):

$$\frac{1}{p^2 - m_R^2 + {\rm i} m_R \Gamma} \left(\frac{\Gamma}{\Gamma_R}\right)^{1/2}, \tag{1}$$

with $\Gamma \to 0$, this way mimicking a delta distribution, i.e., $\delta(p^2 - m_R^2)$. (In the case $X = g$ we had to supplemented the $2 \to 3$ ME for $e^+e^- \to g t\bar{t}$ with the splitting function for $g \to b\bar{b}$.)

In the following, total and differential rates are those at parton level, as we identify jets with the partons from which they originate. Gaussian smearing effects are simulated. No efficiency to tag four b quarks is included.

We start our analysis of the results with a disclaimer: we have not included Initial State Radiation (ISR) [19] in our calculations. We have done so mainly for technical reasons. Simply because we are already dealing with complicated processes requiring delicate integrations, over nineteen dimensions and with a laborious rearrangement of the phase space, to account for the multi-resonant behaviour of hundred of diagrams, that even adding the

ISR in the simplest way[5] would prove rather costly in terms of efficiency of the computation. In addition, we would expect ISR to affect rather similarly the various processes of the form $e^+e^- \to Xb\bar{b}W^+W^- \to b\bar{b}b\bar{b}\ell^\pm\nu_\ell q\bar{q}'$. As we are basically interested in relative rates among the latter, we are confident that the basic features of our results are indifferent to the presence or not of photons radiated by the incoming electron-positron beams[6].

Fig. 4 presents the production cross sections for the following (sub)processes:

1. firstly, the $2 \to 3$ on-shell ones,
$$e^+e^- \to Ht\bar{t}, \tag{2}$$
$$e^+e^- \to Zt\bar{t}, \tag{3}$$
$$e^+e^- \to gt\bar{t}, \tag{4}$$
as obtained from the diagrams in Fig. 1–3 multiplied by the BRs and the $g \to b\bar{b}$ splitting function;

2. secondly, the $2 \to 8$ ones which proceed via those above,
$$e^+e^- \to Ht\bar{t} \to Hb\bar{b}W^+W^- \to b\bar{b}b\bar{b}\ell^\pm\nu_\ell q\bar{q}', \tag{5}$$
$$e^+e^- \to Zt\bar{t} \to Zb\bar{b}W^+W^- \to b\bar{b}b\bar{b}\ell^\pm\nu_\ell q\bar{q}', \tag{6}$$
$$e^+e^- \to gt\bar{t} \to gb\bar{b}W^+W^- \to b\bar{b}b\bar{b}\ell^\pm\nu_\ell q\bar{q}', \tag{7}$$
as obtained from the diagrams in Fig. 1–3 supplemented with the decay currents;

3. thirdly, the $2 \to 8$ ones including also all other diagrams,
$$e^+e^- \to b\bar{b}W^+W^- \to b\bar{b}b\bar{b}\ell^\pm\nu_\ell q\bar{q}', \tag{8}$$
$$e^+e^- \to Zb\bar{b}W^+W^- \to b\bar{b}b\bar{b}\ell^\pm\nu_\ell q\bar{q}', \tag{9}$$
$$e^+e^- \to gb\bar{b}W^+W^- \to b\bar{b}b\bar{b}\ell^\pm\nu_\ell q\bar{q}'. \tag{10}$$

In moving from cases 1. to 2., one can appreciate the onset of spin and width effects, see top of Fig. 4, whereas in comparing 2. and 3. one can disentangle those due to the diagrams not proceeding via X-top-antitop pairs, see bottom of Fig. 4. It turns out that spin and width effects are sizable only for the Higgs-top-antitop and Z-top-antitop processes, not for the gluon-top-antitop ones. They are of the order of $+6\%$ in $Zt\bar{t}$ diagrams, whereas in the case of $Ht\bar{t}$ they vary between $+2.5\%$ at $M_H = 100$ GeV and -15% at $M_H = 140$ GeV. For $gt\bar{t}$ diagrams they amount to less than 1% (hence the overlapping of the two dotted curves in the top frame of Fig. 4). As for effects due to non-X-top-antitop graphs, things go the other way around. The $gt\bar{t}$ rates are hugely increased, by as much as a factor of two, whereas the $Zt\bar{t}$ and $Ht\bar{t}$ ones never get larger than 2.3% and 4.3%, respectively. The growth of the QCD rates is mainly due to the large amount of gluon radiation (here, eventually yielding $b\bar{b}$ pairs) produced in the top quark decays [10]. Note, however, that the latter can easily be controlled by imposing that none of the invariant masses of five particle systems with

[5]For example, via the so-called Electron Structure Function (ESF) approach [19].

[6]We also neglect beamsstrahlung and Linac energy spread, by assuming a narrow beam design [19].

three heavy and two light quarks (and/or two leptons, if the ν_ℓ momentum is reconstructed) reproduces m_t.

Therefore, by studying the production rates of all reactions (2)–(10), one may remark on two key aspects. On the one hand, the bulk of the cross sections of processes (8)–(10) comes from the X-top-antitop channels (5)–(7). On the other hand, the QCD process (7) is the dominant one, for any value of M_H. (That for $M_H \gtrsim 125$ GeV or so the $Zt\bar{t}$ production rates started exceeding the $Ht\bar{t}$ ones was rather trivial to derive [2, 8].) Whereas the first result was clearly expected, the second one came as somewhat of a surprise. As a consequence, in the reminder of our analysis, we will mainly concentrate on the X-top-antitop diagrams and study some of their differential spectra that can help disentangling the Higgs diagrams from the Z and, especially, the gluon ones. We will do so for the choice $M_H = 130$ GeV, as representative of the case in which both Z-top-antitop and gluon-top-antitop backgrounds overwhelm the Higgs-top-antitop signal (see Fig. 4).

As we have already stressed that one of the $b\bar{b}$ pairs in the final state would naturally resonate at M_H, at M_Z or logarithmically increase at low mass, for processes (5), (6) and (7), respectively, we start investigating the di-jet mass spectra that can be reconstructed from the four b quarks in the '$4b + 2$ jets $+\ell^\pm + E_{\rm miss}$' signature. Since we do not assume any jet-charge determination of the (μ-vertex tagged) b jets and consider negligible the mis-tagging of light-quark jets as heavy ones, six such combinations can be built up. We distinguish among these by ordering the four b jets in energy (i.e., $E_1 > E_2 > E_3 > E_4$), in such a way that the $2b$ invariant mass m_{ij} refers to the ij pair (with $i < j = 2, 3, 4$) in which the i-th and j-th most energetic particles enter. Having done so, one should expect to see the typical resonant/logarithmic behaviours described above now 'diluted' in the various ij combinations. This is evident from Fig. 5. There, one can appreciate the resonant shapes around M_H and M_Z in all ij cases (for $ij = 12$, the Z peak is just a tiny kink on top of a Jacobian shape). As for the 'divergence' in the $g \to b\bar{b}$ splitting of the QCD process, this can easily be spotted in the case $ij = 34$. In the end, the $2b$ mass spectra look rather promising as a mean of reducing both backgrounds (6)–(7). By requiring, e.g., $m_{34} > 50$ GeV, one would vigorously reduce the latter; similarly, by imposing, e.g., $|m_{14} - M_Z| > 15$ GeV one would reject the former considerably.

Another way of looking at the same phenomenology in processes (5)–(7) is by studying the energy spectra of the four b quarks. In fact, the larger value of M_H, as compared to M_Z, should boost the b quarks generated by the Higgs boson towards energies higher than those achieved in the Z decays. Conversely, the energy of the b quarks emerging from the two remaining unstable particles, top and antitop quarks, should be softer in the first case. Following similar arguments, one should expect the hardest(softest) b (anti)quark from gluon events to actually be the hardest(softest) of all cases (5)–(7), once again, because of the infrared QCD splitting of a soft gluon. Recalling that the two most energetic b's seldom come from a H, Z or g splitting in $Xb\bar{b}W^+W^-$ intermediate states (see top-left curves in Fig. 5), the above kinematic features are clearly recognisable in Fig. 6. Therefore, the energy spectra too are rather useful in disentangling Higgs events. If one imposes, e.g., $E_1 < 100$ GeV and $E_4 > 50$ GeV, both Z and gluon events can be strongly depleted, at a rather low cost for the signal.

We conclude the numerical analysis by studying the sensitivity of the signal to the Higgs-top Yukawa coupling, by varying the top mass by 5 GeV above and below its default value.

$\sigma_{\rm tot}$ (fb)			
m_t (GeV)	$HbbW^+W^-$	$ZbbW^+W^-$	$gbbW^+W^-$
170	0.061	0.087	0.79
175	0.033	0.067	0.77
180	0.012	0.050	0.74

Table 1: Cross sections for processes (see the text) (8)–(10), for three discrete values of the top mass. The total CM energy is $\sqrt{s} \equiv E_{\rm cm} = 500$ GeV. The Higgs boson mass is $M_H = 130$ GeV. No cuts have been implemented. (Numerical errors from the Monte Carlo integration do not affect the significant digits shown.)

However, as to modify m_t (and, consequently, Γ_t) has also incidence on the top propagators, and since these enter many of the diagrams associated with processes (8)–(10), we present the rates for the latter, that is, for the full sets of diagrams in each case. This is done in Tab. 1. The value we have chosen for the Higgs mass, i.e., $M_H = 130$ GeV, is a critical one for process (5), the main source of events (8). In the sense that the sum $2m_t + M_H$ is very close to $\sqrt{s}$, so that the corresponding rates in Tab. 1 (see second column) are the result of the interplay between the rise of the cross section with m_t^2 and its fall because of the phase space suppression (width effects are less relevant). Indeed, between the two tendencies is the latter to dominate. In fact, the production cross sections of all three processes (8)–(10) decrease with increasing top mass. Even in presence of such delicate interplay, the sensitivity of Higgs-top-antitop events to the actual value of the top mass is rather strong, as the corresponding cross section changes by a factor of 5 between $m_t = 170$ and 180 GeV. Backgrounds variations are always smaller. However, both processes (9)–(10) are larger than (8). Once again, it has to be stressed that background rates ought to be reduced severely if one wants to perform dedicated studies of the Higgs-top Yukawa coupling.

In summary, in our opinion, the study of the Higgs-top Yukawa coupling at future electron-positron colliders, such as the NLC running with a CM energy of 500 GeV, can in principle be pursued by means of the Higgs-strahlung process $e^+e^- \to Ht\bar{t}$. In fact, the irreducible backgrounds affecting the latter can be brought under control in the semi-leptonic top-antitop decay channel $t\bar{t} \to b\bar{b}W^+W^- \to b\bar{b}\ell^\pm\nu_\ell q\bar{q}'$, further assuming $H \to b\bar{b}$, as natural for Higgs masses up to 140 GeV or so.

However, this requires to somehow recognise the b jets in the final state with high efficiency, as the observable rates of the signal are below the femtobarn level. The knowledge of the momenta of the heavy quark jets entering the signature '$4b+2$ jets $+\ell^\pm + E_{\rm miss}$' is crucial in order to reduce the overwhelming QCD background, mainly proceeding via $e^+e^- \to gt\bar{t}$ events, if one aims to disentangle such Higgs events at all. The competing electroweak background, mainly proceeding through $e^+e^- \to Zt\bar{t}$ intermediate states, can be dealt with if the mass resolution of di-jet pairs of b quarks is around 10 GeV or less. Other irreducible background channels, induced by $e^+e^- \not\to Xt\bar{t} \to Xb\bar{b}\ W^+W^-$ intermediate states, with $X = H, Z$ or g, are significantly smaller than those proceeding via X-top-antitop graphs, with the only exception of QCD graphs involving one radiative (anti)top decay.

In the end then, although a careful simulation of possible tagging strategies should eventually be performed, we believe that, if the Higgs mass turns out to be in the intermediate range, the NLC constitutes an ideal laboratory for the kind of studies sketched here. We

base our conviction on the fact the we have performed a new and rather complete calculation of signal and backgrounds involving up to ten external particles.

References

[1] Proceedings of the Workshop e^+e^- *Collisions at 500 GeV. The Physics Potential*, Munich, Annecy, Hamburg, 3–4 February 1991, ed. P.M. Zerwas, DESY 92–123A/B, August 1992, DESY 93–123C, December 1993.

[2] A. Djouadi, J. Kalinowski and P.M. Zerwas, *Mod. Phys. Lett.* **A7** (1992) 1765; *Z. Phys.* **C54** (1992) 255.

[3] See, e.g.: Section 'Top Quark Physics', P. Igo-Kemenes and J.H. Kühn (conveners), in Ref. [1] (and references therein), part A.

[4] Z. Kunszt, S. Moretti and W.J. Stirling, *Z. Phys.* **C74** (1997) 479.

[5] W. Bernreuther *et al.*, in Ref. [1], part A.

[6] G. Bagliesi *et al.*, in Ref. [1], part A.

[7] K.J.F. Gaemers and G.J. Gounaris, *Phys. Lett.* **B77** (1978) 379.

[8] K. Hagiwara, H. Murayama and T. Watanabe, *Nucl. Phys.* **B367** (1991) 257.

[9] See, e.g.: LEP Higgs Working Group, http://www.cern.ch/LEPHIGGS/.

[10] L.H. Orr, T. Stelzer and W.J. Stirling, *Phys. Lett.* **B354** (1995) 442.

[11] S. Dawson and L. Reina, *Phys. Rev.* **D57** (1998) 5851; preprint MADPH-98-1073, FSU-HEP-980812, BNL-HET-98-27, August 1998, `hep-ph/9808443`; S. Dittmaier, M. Krämer, Y. Liao, M. Spira and P. M. Zerwas, *Phys. Lett.* **B441** (1998) 383.

[12] H. Murayama, I. Watanabe and K. Hagiwara, HELAS: HELicity Amplitude Subroutines for Feynman Diagram Evaluations, *KEK Report* 91-11, January 1992.

[13] K. Hagiwara and D. Zeppenfeld, *Nucl. Phys.* **B274** (1986) 1.

[14] F.A. Berends, P.H. Daverveldt and R. Kleiss, *Nucl. Phys.* **B253** (1985) 441; R. Kleiss and W.J. Stirling, *Nucl. Phys.* **B262** (1985) 235.

[15] S. Moretti, *Phys. Rev.* **D50** (1994) 2016.

[16] A. Ballestrero, E. Maina and S. Moretti, *Phys. Lett.* **B335** (1994) 460; S. Moretti, *Phys. Rev.* **D50** (1995) 6316; *Z. Phys.* **C73** (1997) 653; S. Moretti and K. Odagiri, *Eur. Phys. J.* **C1** (1998) 633.

[17] G.P. Lepage, *Jour. Comp. Phys.* **27** (1978) 192.

[18] R. Kleiss, W.J. Stirling and S.D. Ellis, *Comput. Phys. Commun.* **40** (1986) 359.

[19] T. Barklow, P. Chen and W. Kozanecki, in Ref. [1], part A.

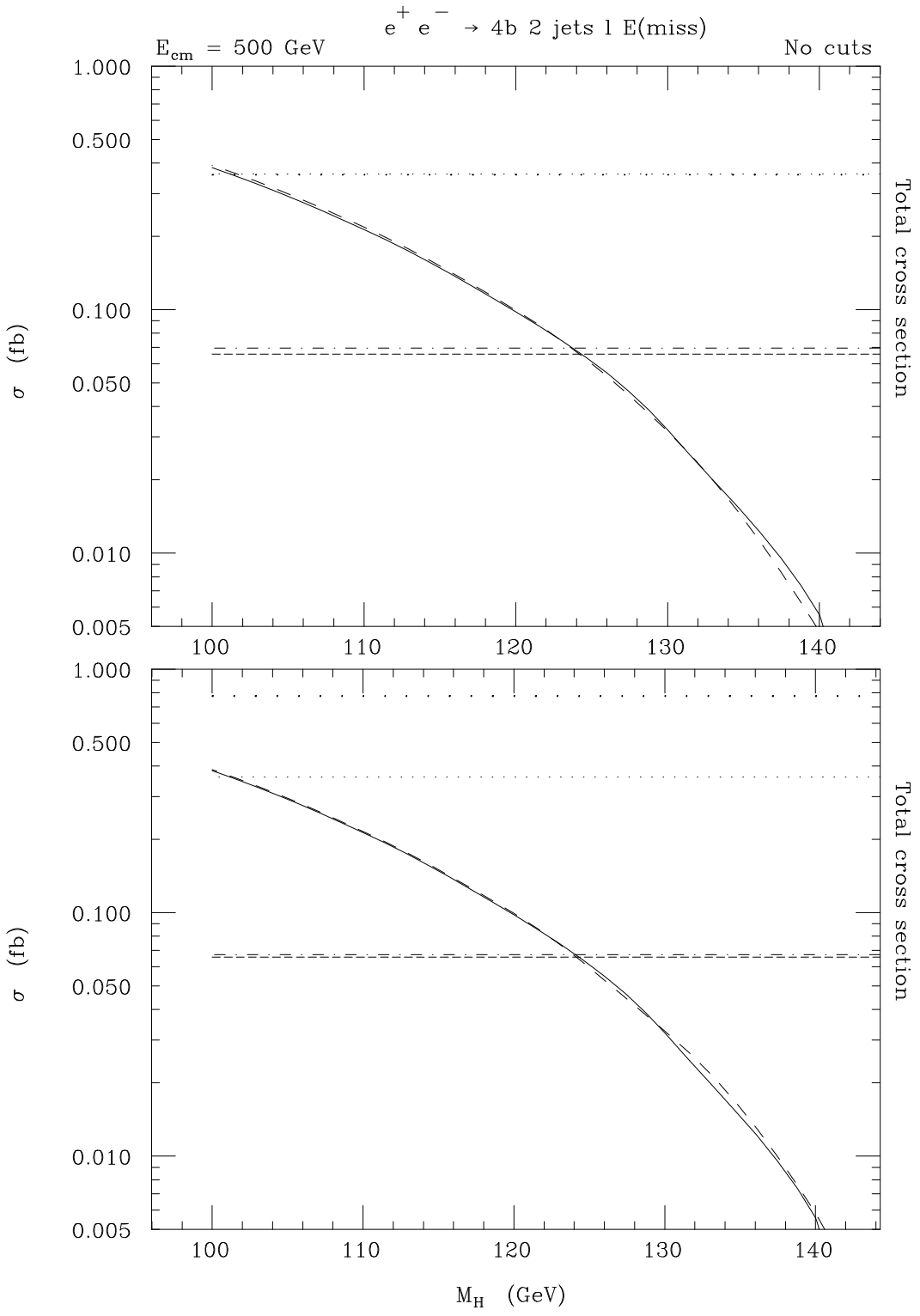


Figure 4: Cross sections for the following processes (see the text): (2) (long-dashed line, above), (3) (dot-dashed line, above) and (4) (dotted line, above); (5) (solid line, above and below), (6) (dashed line, above and below) and (7) (fine-dotted line, above and below); (8) (long-dashed line, below), (9) (dot-dashed line, below) and (10) (dotted line, below). The total CM energy is $\sqrt{s} \equiv E_{\rm cm} = 500$ GeV. No cuts have been implemented.

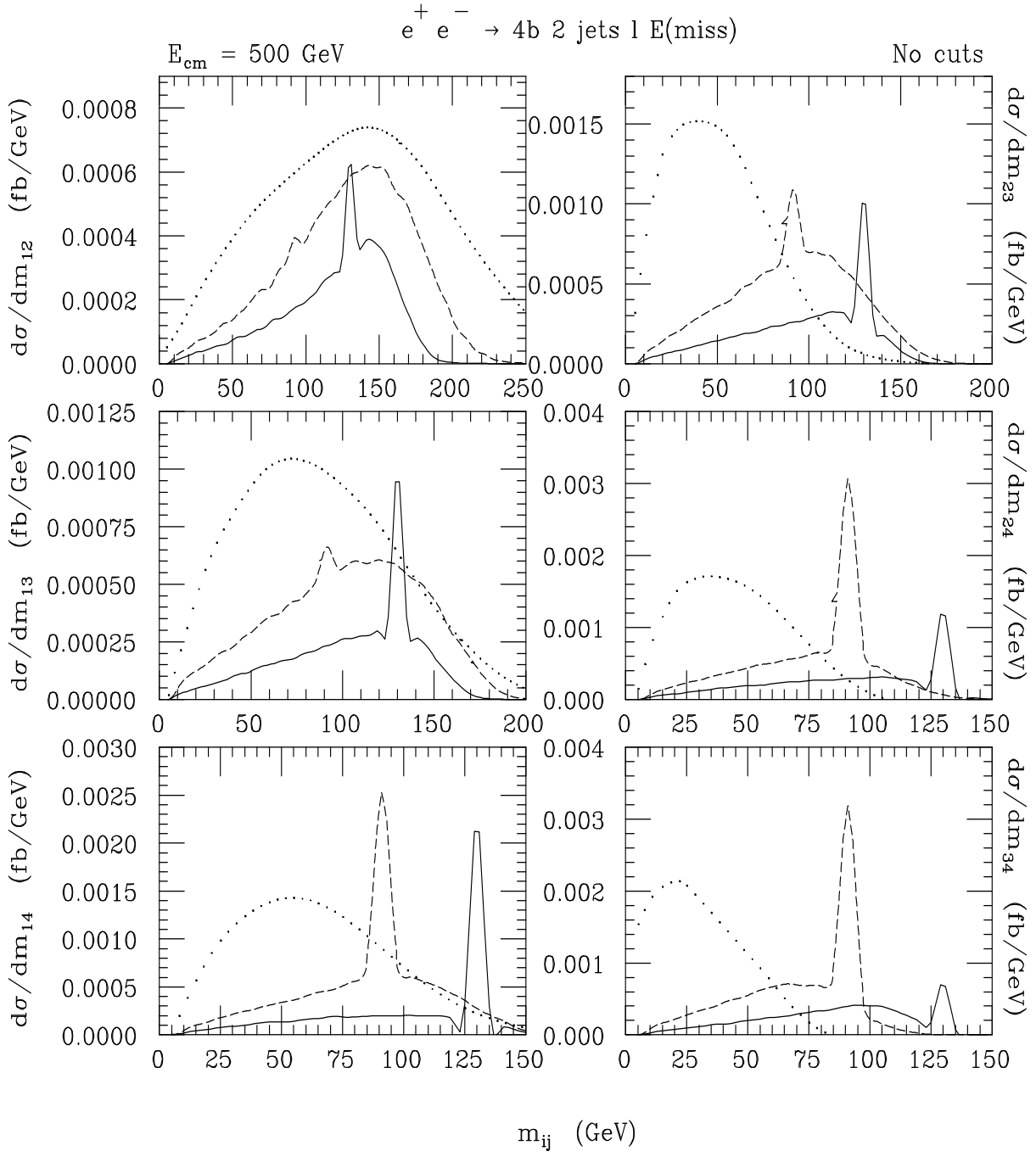


Figure 5: Differential distributions in the invariant mass of all possible combinations ij, with $i < j = 2, ...4$, of the energy-ordered b jets (i.e., such that $E_1 > E_2 > E_3 > E_4$) for the following processes (see the text): (5) (solid line), (6) (dashed line) and (7) (dotted line). The total CM energy is $\sqrt{s} \equiv E_{\rm cm} = 500$ GeV. No cuts have been implemented. Note that the rates of reaction (7) have been divided by three for readability.

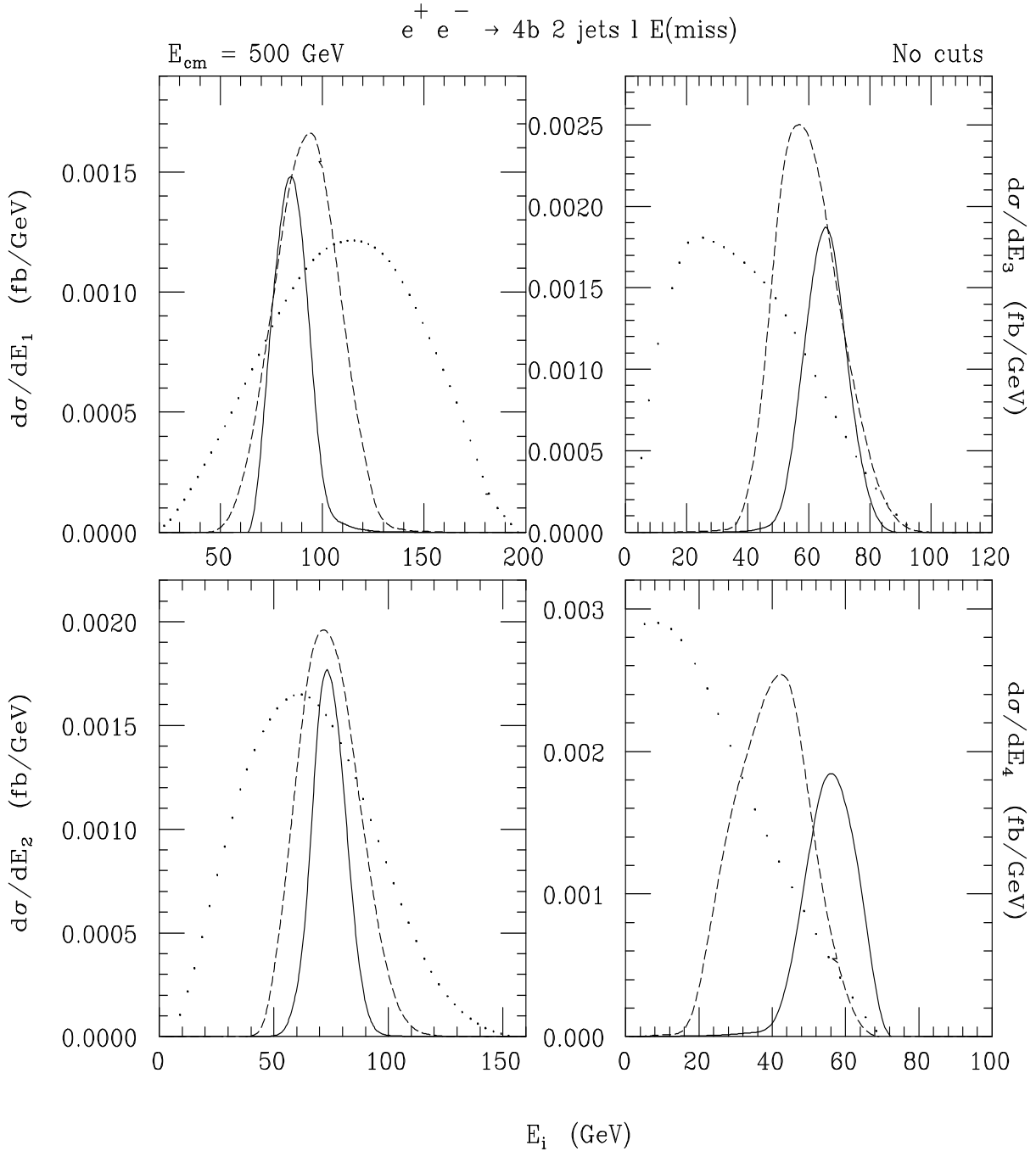


Figure 6: Differential distributions in energy of the energy-ordered b jets (i.e., such that $E_1 > E_2 > E_3 > E_4$) for the following processes (see the text): (5) (solid line), (6) (dashed line) and (7) (dotted line). The total CM energy is $\sqrt{s} \equiv E_{\rm cm} = 500$ GeV. No cuts have been implemented. Note that the rates of reaction (7) have been divided by three for readability.